VIII. ELECTRODYNAMICS OF MEDIA

Academic Research Staff

Prof. Hermann A. Haus
Prof. Jin-Au Kong
Prof. Paul L. Penfield, Jr.
Prof. David H. Staelin
Prof. Abraham Szöke

Graduate Students

Donald L. Lee
Monica Minden
Eni G. Njoku
Edward M. Singel
Leung Tsang
John C. Ufford

A. COMPARISON OF THE HORIZONTAL MAGNETIC DIPOLE WITH THE HORIZONTAL ELECTRIC DIPOLE IN GEOPHYSICAL SUBSURFACE PROBING

JSEP

Joint Services Electronics Program (Contract DAAB07-74-C-0630)

Wing-Cheung Chan, Jin-Au Kong, Leung Tsang

The use of a horizontal electric dipole (HED) in geophysical subsurface probing with the electromagnetic interference fringes method has been studied extensively.[1,2] In this report similar calculations are performed for a horizontal magnetic dipole (HMD) by using the reflection coefficient formulation[3] and the saddle-point method, and the calculations are compared with those obtained for a horizontal electric dipole.

The radiation patterns in the broadside direction are compared in Fig. VIII-1. The angle at which the coupling power is maximum occurs at the critical angle $\sin^{-1}(1/n)$, where n is the refractive index of the half-space medium. The radiation patterns in the end-fire direction are compared in Fig. VIII-2. It is found that the angle of maximum

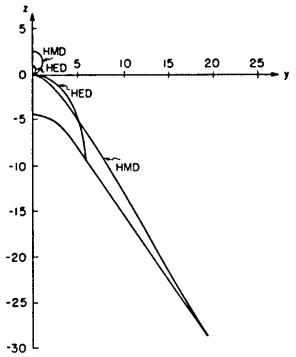

Fig. VIII-1.

Radiation pattern for HMD and HED at ϕ = 90°. (Values for HED from Tsang and Kong.[2]) HMD: $\epsilon_1 = 3.2$. HED: $\epsilon_1 = 3.3$.

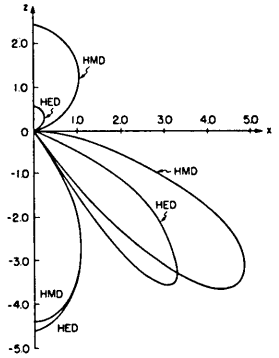

Fig. VIII-2.

Radiation pattern for HMD and HED at ϕ = 0. (Values for HED from Tsang and Kong.[2]) HMD: $\epsilon_1 = 3.2$. HED: $\epsilon_1 = 3.5$.

JSEP

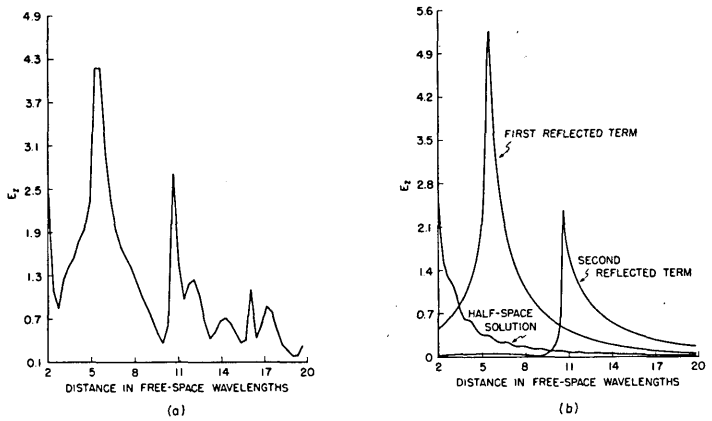

Fig. VIII-3. (a) Interference pattern for E_z.
$\epsilon_1 = 3.3$ $\quad d = 4\lambda$
$\epsilon_2 = 500i$ $\quad LT = 0.005$
(b) Comparison of the half-space solution with the reflected terms.
$\epsilon_1 = 3.3$ $\quad d = 4\lambda$
$\epsilon_2 = 500i$ $\quad LT = 0.005$

Table VIII-1. Comparison of HED and HMD.

	HED	HMD
Field Components		
Broadside	$H_z^{TE}, E_\phi^{TE}, H_\rho^{TE}$	$E_z^{TM}, H_\phi^{TM}, E_\rho^{TM}$
End fire	$E_z^{TM}, H_\phi^{TM}, E_\rho^{TM}$	$H_z^{TE}, E_\phi^{TE}, H_\rho^{TE}$
Radiation Pattern		
Upper medium	$\frac{3}{2}\left[x_{o1}^2(\theta)\sin^2\phi + y_{1o}^2(\theta)\cos^2\theta\cos^2\phi\right]$	$\frac{3}{2}\left[y_{o1}^2(\theta)\sin^2\phi + x_{1o}^2(\theta)\cos^2\theta\cos^2\phi\right]$
Lower medium	$\frac{3}{2}\left[\lvert x_{1o}^2(\alpha)\rvert^2\sin^2\phi + \lvert y_{o1}(\alpha)\rvert^2\cos^2\alpha\cos^2\phi\right]$	$\frac{3}{2}\left(\frac{\mu_1\epsilon_1^3}{\mu_o\epsilon_o^3}\right)^{1/2}\left[\lvert y_{1o}(\alpha)\rvert^2\sin^2\phi + \lvert x_{o1}(\alpha)\rvert^2\cos^2\alpha\cos^2\phi\right]$
Broadside angle	$\sin^{-1}(1/n)$	$\sin^{-1}(1/n)$
End-fire angle	$\sin^{-1}\left(\frac{2}{1+n^2}\right)^{1/2}$	$\sin^{-1}\left(\frac{1+n^2}{2n^2}\right)^{1/2}$

power coupling for the HMD occurs at $\sin^{-1}\sqrt{2/(1+n^2)}$, while for the HED it occurs at $\sin^{-1}\sqrt{(1+n^2)/2n^2}$. Thus for the HMD this angle ranges from 0 to 90°, while for the HED it only spans 0-45°. JSEP

Figure VIII-3a shows an interference pattern for E_z for a highly reflecting subsurface situated 4 free-space wavelengths below the surface. The occurrence of the high peak is illustrated by the first reflected term in Fig. VIII-3b, which evidently is due to the power launched into medium 1 at the critical angle.

In Table VIII-1, the corresponding field components in the broadside and end-fire directions are listed. The formulas used in calculating the radiation patterns are also compared.

The implication of these results is that the HMD may be more effective in subsurface probing than the HED. In the broadside direction power is more concentrated at the critical angle; hence, there is a sharper peak in the interference pattern. Note that these calculations are performed for a horizontal magnetic dipole on the surface of the probing area. In actual experiments, the HMD may have to be elevated. By using the reflection coefficient formulation and similar techniques, field components can be calculated in detail.

References

1. J. A. Kong, L. Tsang, and G. Simmons, "Geophysical Subsurface Probing with Radio-Frequency Interferometry," IEEE Trans., Vol. AP-22, No. 4, pp. 616-620, July 1974.
2. L. Tsang and J. A. Kong, "Interference Patterns of a Horizontal Electric Dipole over Layered Dielectric Media," J. Geophys. Res. 78, 3287-3300 (1973).
3. J. A. Kong, "Electromagnetic Fields Due to Dipole Antennas over Stratified Anisotropic Media," Geophys. 37, 985-996 (1972).

B. EFFECTS OF SCATTERING AND NONUNIFORM TEMPERATURE DISTRIBUTIONS ON BRIGHTNESS TEMPERATURE IN REMOTE SENSING

Joint Services Electronics Program (Contract DAAB07-74-C-0630)

Leung Tsang, Jin-Au Kong

In passive remote sensing of the Earth with microwaves, the brightness temperature reading of a radiometer depends on its angle of observation and on the microwave emissive properties of the observed area. Various theories have been developed for interpretation of data collected from satellites and spacecraft, with a half-space dielectric medium used as the model. It is well understood that in snow, ice, or desert areas the subsurface temperature profile, absorption, and scattering are dominant factors in the JSEP

JSEP surface-brightness temperature.[1,2] Assuming uniform temperature distribution, Gurvich and his co-workers derived expressions for the brightness temperatures of a half-space random medium with a laminar structure.[3] Using a radiative transfer approach, England[4] considered a nonuniform temperature profile and assumed an isotropic scattering phase function. Stogryn[5] examined the brightness temperature of a vertically structured medium with no scattering. Using a perturbation approach,[6] he also studied scattering by random dielectric constant fluctuations in the low-frequency limit. In this report we solve the problem of microwave thermal emission from a half-space medium with a laminar structure and nonuniform temperature profile by using the radiative transfer approach.

For a half-space medium with constant absorption and scattering coefficients, the brightness temperature is determined by the following simple closed-form formula[7]

$$T_B = \frac{2\kappa_a(1-r_{ot})}{(a+\kappa_a) - r_{ot}(a-\kappa_a)} \left\{T_o + \frac{a}{a+\gamma\cos\theta} T_h\right\}, \tag{1}$$

where we assume that the temperature distribution has the profile

$$T(z) = T_o + T_h e^{\gamma z}. \tag{2}$$

In (1) r_{ot} is the reflectivity of the medium, θ the observation angle, κ_a the absorption coefficient, and

$$a = (\kappa_a+\kappa_s)\sqrt{(1-\tilde{\omega})\left[1 - \frac{\tilde{\omega}}{2}P_f + \frac{\tilde{\omega}}{2}P_b\right]}. \tag{3}$$

In (3) κ_s is the scattering coefficient, P_f the forward-scattering function, P_b the backward-scattering function, and the scattering albedo is

$$\tilde{\omega} = \frac{\kappa_s}{\kappa_a + \kappa_s}. \tag{4}$$

We shall now examine several special cases.

(a) For a medium with uniform temperature distribution and no scattering, $T_h = 0$, $\kappa_s = 0$, and $a = \kappa_a$. Thus

$$T_B = (1-r_{ot})T_o. \tag{5}$$

The emissivity is seen to be given by $1 - r_{ot}$. This result also agrees with that obtained by reciprocity arguments.

(b) For a medium with no scattering, $\kappa_s = \tilde{\omega} = 0$. Thus

$$T_B = (1-r_{ot})\left(T_o + \frac{\kappa_a T_h}{\kappa_a + \gamma\cos\theta}\right). \tag{6}$$

JSEP

As a numerical example, we consider the subsurface temperature distribution of the Amundsen-Scott Station in Antarctica.[8] The temperature profile is first fitted with exponentials. For April 1, 1958, we find that $T(z) = 222 + 81\, e^{0.51z} - 88\, e^{0.66z}$. The brightness temperatures as a function of frequency at the nadir are shown in Fig. VIII-4 for

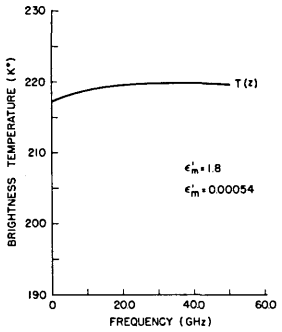

Fig. VIII-4.

Brightness temperature without scattering as a function of frequency for the temperature distribution at the Amundsen-Scott Station in Antarctica.

$\epsilon_m = 1.8(1 + i0.003)\,\epsilon_o$. It is seen that at very low frequencies T_B is determined by the temperature at greater depth, which is essentially a constant $T_o = 222°K$, with the emissivity of ice surface approximately e = 0.978. As the frequency increases, the subsurface temperature becomes more important. At very high frequencies the brightness temperature approaches the value $e(T_o + T_h)$, as seen from (6).

(c) For a medium with scattering and uniform temperature distribution, $T_h = 0$. Thus we find

$$T_B = \frac{2\kappa_a(1-r_{ot})}{(a+\kappa_a) - r_{ot}(a-\kappa_a)}\, T_o. \tag{7}$$

Numerical results are presented in Figs. VIII-5 and VIII-6 and compared with those obtained by Gurvich et al.[3] We see that for the Shelf glacier (Fig. VIII-5), higher brightness temperatures are predicted with our model. The reason is that Gurvich's results are applicable to small-scattering cases, whereas the scattering albedo for the Shelf glacier is rather large. For the Continental glacier (Fig. VIII-6) where the scattering albedo is quite small, both models agree quite well except at resonance where the scattering is largest.

(d) For uniform temperature distribution and small scattering albedo, we expand (7) to first order in $\tilde{\omega}$ cast in a form to compare it with the results obtained by Gurvich et al.

JSEP

$$T_B = (1-r_{ot})\left(1 - \frac{(1-r_{ot})k_m^2 \Delta \ell}{8k_m'' \cos\theta\left(1 + 4k_m^2 \ell^2 \cos^2\theta\right)}\right) T_o. \tag{8}$$

This expression differs from their result, since they have $\cos\theta_o$ in the numerator instead of $\cos\theta$ in the denominator as shown in (8). By using the wave approach,[7] we have an alternative derivation that confirms (8).

Numerical results are given in Fig. VIII-7 to compare brightness temperature for

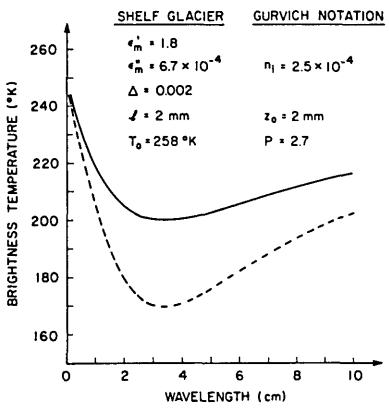

Fig. VIII-5.

Brightness temperature for the Shelf glacier (solid line) compared with that obtained by Gurvich et al. (broken line).

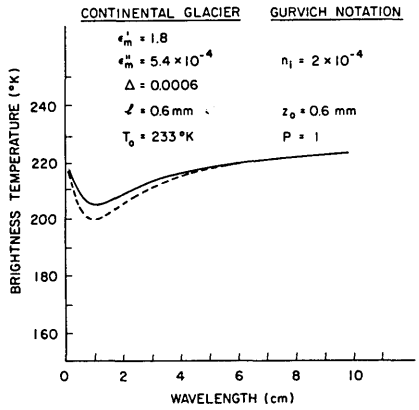

Fig. VIII-6.

Brightness temperature for the Continental glacier (solid line) compared with that obtained by Gurvich et al. (broken line).

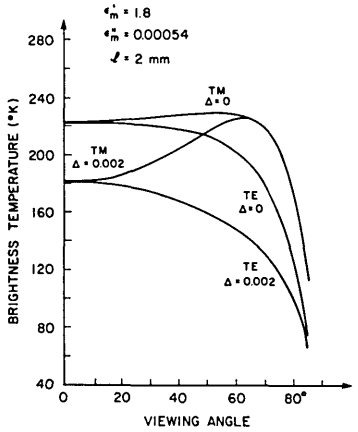

Fig. VIII-7. Brightness temperature as a function of radiometer viewing angle for TE and TM waves. (Frequency 20 GHz.)

JSEP

TE and TM waves as a function of radiometer viewing angle θ_o, with temperature profile JSEP
$T(z) = 222 + 34 \exp[0.81z]$. Clearly, scattering lowers the brightness temperature at all viewing angles.

References

1. J. A. Kong, "Microwave Remote Sensing of Ice and Snow," Proc. URSI Commission II Specialist Meeting on Microwave Scattering and Emission from the Earth, September 24, 1974, pp. 239-243.
2. K. F. Kunzi, D. H. Staelin, and J. W. Waters, "Earth Surface Emission Measured with the Nimbus-5 Microwave Spectrometer," Proc. URSI Commission II Specialist Meeting on Microwave Scattering and Emission from the Earth, September 24, 1974, p. 113.
3. A. S. Gurvich, V. I. Kalinin, and D. T. Matveyev, "Influence of the Internal Structure of Glaciers on Their Thermal Radio Emission," Atm. and Oceanic Phys. 9, 712-717 (1973).
4. A. W. England, "Thermal Microwave Emission from a Halfspace Containing Scatterers," Radio Sci. 9, 447-454 (1974).
5. A. Stogryn, "The Brightness Temperature of a Vertically Structured Medium," Radio Sci. 5, 1397-1406 (1970).
6. A. Stogryn, "Electromagnetic Scattering by Random Dielectric Constant Fluctuations in a Bounded Medium," Radio Sci. 9, 509-518 (1974).
7. L. Tsang and J. A. Kong, "The Brightness Temperature of a Half-Space Random Medium with Nonuniform Temperature Profile," Electrodynamics Memo 42, Research Laboratory of Electronics, M.I.T., May 7, 1975.
8. H. Lettau, "Antarctic Atmosphere as a Test Tube for Meteorological Theories," in Research in the Antarctic (American Association for the Advancement of Science, Washington, D. C., 1971), pp. 443-475. JSEP

JSEP

C. INTERPRETATION OF REMOTE SENSING DATA

Joint Services Electronics Program (Contract DAAB07-74-C-0630)

Masato Nagase, Donald Chu

A two-layer model[1] has been used to match microwave emission data of fresh water ice and snow as measured by Schmugge et al.[2] The emissivity of the two-layer medium is governed by seven parameters: d, ϵ_1', ϵ_1'', ϵ_2', ϵ_2'', z_o, and P, where $\epsilon_1 = \epsilon_1' + i\epsilon_1''$ and $\epsilon_2 = \epsilon_2' + i\epsilon_2''$ are the complex dielectric constants of the top and the bottom layers, d is the thickness of the top layer, z_o is a characteristic correlation depth of the refractive index $n = n_1' + in_1'' = (\epsilon_1' + i\epsilon_1'')^{1/2}$ of the top layer, and P is related to the variance σ_{no}^2 by $P = (n_1'/n_1'')\sigma_{no}^2$.

Table VIII-2. Emissivity of the two-layer medium.

	Bear Lake	Steamboat Lake	South Cascade Lake
d m	0.15	0.8	0.5
ϵ_1'	3.2	2.2	2.9-3.2
ϵ_1''	0.04-0.048	0.04	0.095-0.11
ϵ_2'	80	60-80	70-80
ϵ_2''	80	0-80	0-20
P	1.1-1.6	1.34-1.38	0.35-0.45
z_o mm	0.8-1.2	0.37-0.4	0.5-0.65

	S.C. Glacier, P-3	S.C. Glacier, P-1	S.C. Glacier, P-0
d m	8.4	6.8	4.9
ϵ_1'	3.1	2.7-2.8	2.6-2.7
ϵ_1''	0-0.0004	0-0.0004	0-0.0008
ϵ_2'	3.0-3.2	3.1-3.2	3.0-3.2
ϵ_2''	0.004-0.05	0.004-0.05	0.03-0.05
P	1.8-2.1	1.9-2.0	1.75-2.3
z_o mm	0.75-0.9	0.9-0.95	0.5-0.8

JSEP

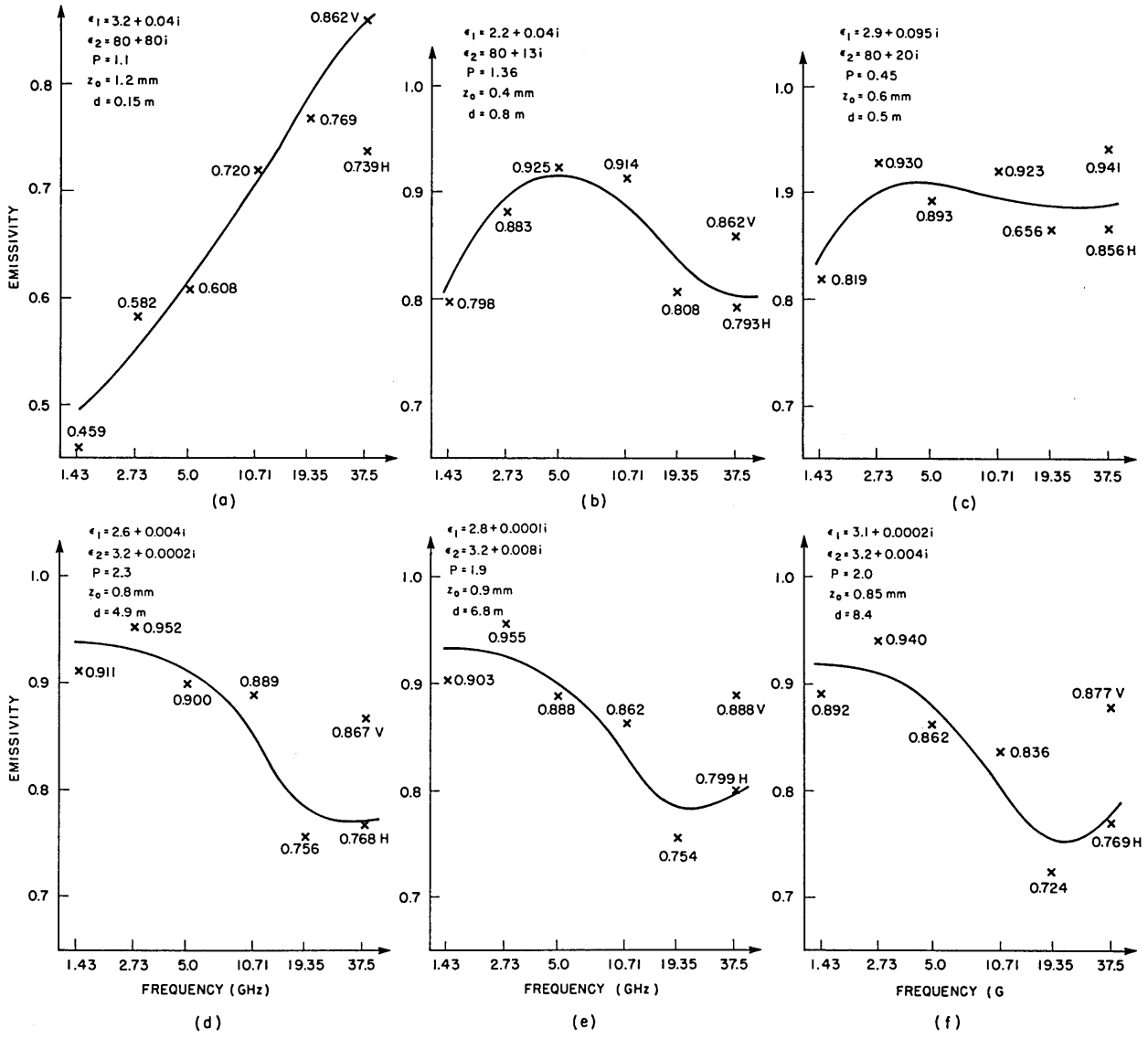

Fig. VIII-8. Results of matching microwave emission data of fresh water ice and snow. (a) Bear Lake, (b) Steamboat Spring, (c) South Cascade Lake, (d) South Cascade Glacier, P-0, (e) South Cascade Glacier, P-1, (f) South Cascade Glacier, P-3.

JSEP

The remote sensing data are matched by inspection and by an automatic inversion scheme, implemented with the MACSYMA computer system. The results are illustrated in Fig. VIII-8 and summarized in Table VIII-2. They agree quite well with ground truth measurements.

References

1. J. A. Kong, "Microwave Remote Sensing of Ice and Snow," Proc. URSI Commission II, E. Schanda (Ed.), Institute of Applied Physics, University of Bern, Switzerland, 1974.

2. T. Schmugge, T. T. Wilheit, P. Gloersen, M. F. Meier, D. Frank, and I. Dirmhirm, "Microwave Signatures of Snow and Fresh Water Ice," presented at the Interdisciplinary Symposium on Advanced Concepts and Techniques in the Study of Snow and Ice Resources (Goddard Space Flight Center, Greenbelt, Maryland, November 1973).

JSEP

D. CALCULATION OF THE BRIGHTNESS TEMPERATURE OF AN INHOMOGENEOUS MEDIUM WITH THE FLUCTUATION-DISSIPATION APPROACH

California Institute of Technology (Contract 953524)

Leung Tsang, Eni G. Njoku, Jin-Au Kong

With the fluctuation-dissipation approach we calculate the brightness temperature of a stratified medium with inhomogeneous permittivities and nonuniform temperature, using a stratified model expressed in the following form:

$$T_B(\bar{k},\omega) = k^3 \cos\theta \sum_{\ell=1}^{t} \frac{\epsilon_\ell''}{\epsilon_o} \int_{-d_\ell}^{-d_{\ell-1}} dz'\, T_\ell(z') \left\{ \left| \frac{1}{k_z} \hat{e}(k_z) \left[A_\ell \hat{e}_\ell(-k_{\ell z})\, e^{ik_{\ell z} z'} + B_\ell \hat{e}_\ell(k_{\ell z})\, e^{-ik_{\ell z} z'} \right] \right|^2 + \left| \frac{1}{k_z} \hat{h}(k_z) \left[C_\ell \hat{h}_\ell(-k_{\ell z})\, e^{ik_{\ell z} z'} + D_\ell \hat{h}_\ell(k_{\ell z})\, e^{-ik_{\ell z} z'} \right] \right|^2 \right\}, \tag{1}$$

where

$$\hat{e}_\ell(k_z) = \frac{1}{\left(k_x^2 + k_y^2\right)^{1/2}} \{\hat{x} k_y - \hat{y} k_x\} \tag{2}$$

$$\hat{h}_\ell(k_z) = \frac{1}{k_\ell} \{\hat{e}_\ell \times \bar{k}_\ell\}. \tag{3}$$

Here e is the observation angle, ϵ_ℓ'' is the imaginary part of the permittivity in layer ℓ, $T_\ell(z')$ is the temperature distribution in layer ℓ, and A_ℓ, B_ℓ, C_ℓ, and D_ℓ are wave amplitudes in region ℓ that are related to those in other regions by propagation matrices.[1]

In Fig. VIII-9 the brightness temperature as observed from the nadir is plotted as a function of frequency for the following profiles:

$$\epsilon_1(z) = 9.0(1+i0.1) - (5.5+i0.83)\, e^{az}$$

$$\epsilon_t(z<-20 \text{ cm}) = 9.0(1+i0.05)$$

$$T(z) = T_o + \Delta T\, e^{bz}$$

$$T_t = T(z=-20 \text{ cm})$$

with $a = 0.02 \text{ cm}^{-1}$, $b = 0.1 \text{ cm}^{-1}$, $T_o = 280°K$, and $\Delta T = 20°K$. Note that there is an abrupt change in the permittivity profile at $z = -20$ cm. At low frequency there is

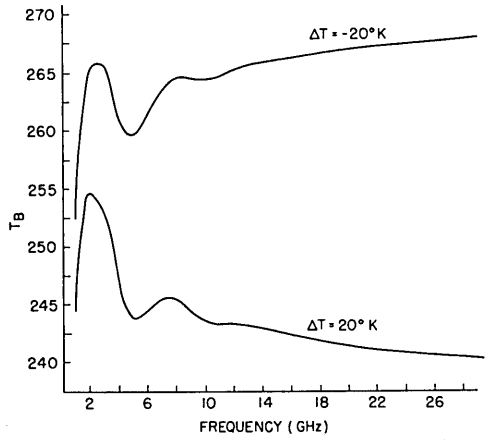

Fig. VIII-9.
Brightness temperature as a function of frequency.

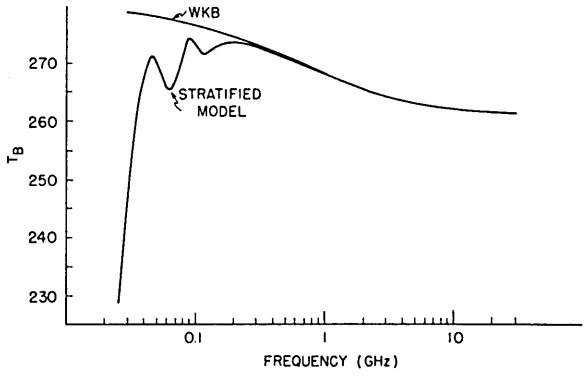

Fig. VIII-10. Brightness temperature calculated with the stratified model and compared with the WKB result.

interference. In Fig. VIII-10 we illustrate the brightness temperature from the nadir calculated for the following profiles:

$$\epsilon_1(z) = (2.88+i0.34)\, e^{-az}$$

$$\epsilon_t = \epsilon_1(z=-1\ \text{m})$$

$$T(z) = 300 - 20\, e^{bz} \quad \text{for } -\infty < z < 0,$$

with $a = 2\ \text{m}^{-1}$ and $b = 3\ \text{m}^{-1}$. The result calculated with the stratified model is found to agree very well with that calculated with the exact formulas for this case.

When the permittivity profile is smooth enough that the WKB approach[2] is valid, the brightness temperature can also be calculated and expressed in the following form:

$$T_h = (1-r^{TE}) \int_{-\infty}^{0} dz\, 2T(z)\, \frac{|g(0)|}{|g(z)|}\, \frac{g'(z)}{g'(0)}\, g''(z) \exp\left[2 \int_0^z ds\, g''(s)\right] \tag{4}$$

$$T_v = (1-r^{TM}) \int_{-\infty}^{0} dz\, 2T(z)\, \frac{f(z)}{f(0)}\, \frac{|g(0)|}{|g(z)|}\, \frac{g'(z)}{g'(0)}\, g''(z) \exp\left[2 \int_0^z ds\, g''(s)\right], \tag{5}$$

where

$$g^2(z) = \epsilon_r k^2 - k_x^2 - k_y^2 = (g'(z)+ig''(z))^2$$

$$f(z) = \frac{|g(z)|^2 + k_x^2 + k_y^2}{|\epsilon_r(z)|}.$$

Here r^{TM} is the reflectivity for horizontally polarized waves, r^{TE} is the reflectivity for vertically polarized waves, and $\epsilon_r(z)$ is the dielectric constant of the inhomogeneous medium. To illustrate the use of (4) and (5), we plot the WKB result in Fig. VIII-10 to compare it with that obtained from the stratified model. We note that the WKB result is quite accurate on the high-frequency side where the CPU time with WKB is also less as compared with the stratified method.

References

1. J. A. Kong, "Reflection and Transmission of Electromagnetic Waves by Stratified Moving Media," Can. J. Phys. 49, 2786-2797 (1971).

2. A. Stogryn, "The Brightness Temperature of a Vertically Structured Medium," Radio Sci. 5, 1397-1406 (1970).